1 Introduction

1.1 Space debris

Space debris, as the name suggests, is any artificial object in orbit about the Earth that is non-functional or the product of impact, explosion, the product of satellite deployment, but otherwise not directly related to a space mission. As such, it consists of bodies occupying a wide range of size and mass, from spent rocket stages and defunct satellites in the many-metre, many tonne region, down through the sub-metre range such as fasteners, straps, mylar thermal shielding, astronaut equipment, unsalvageable satellite parts (HST solar array, still in orbit, and the SFU (Space Flyer Unit) solar array, down to the millimetric range: impact/explosion fragments, explosive bolts, fasteners, solid rocket motor exhaust, and paint flakes (Johnson & McKnight, 1987), (Klinkrad, 1998).

Until 1957, the debris environment about the Earth consisted solely of naturally-occurring meteoroids in solar orbit. After the launch of Sputnik 1 in October 1957 however, the number of debris particles in Earth orbit has increased steadily. See Figure 1.1; from Johnson & McKnight, 1987.

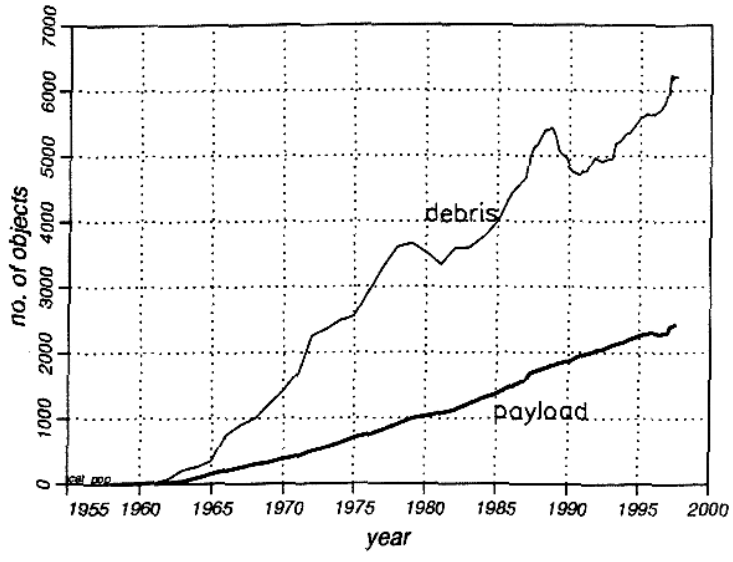

Figure 1.1: Debris particle population growth since the beginning of the space age.

The danger posed by the debris environment comes from the high relative velocities involved on impact of approx. 10 km s^{-1}. At such speeds the damage caused by small particles can have disastrous effects on the functioning of a

satellite or the habitability of a space station - the International Space Station is armoured against impact by debris up to 1cm in diameter (Beruto *et al*, 1997).

1.1.1 Debris sources and sinks

The debris population in Earth orbit is governed by a variety of sources and sinks, which are listed here:

Sources

- Standard orbital activity: explosive bolts are used to separate stages; despin yo-yos that are discarded after use; used upper stage rocket bodies; solid rocket motor exhaust; escaped coolant from nuclear-powered satellites (Stansberry *et al*, 1997); routine exhaust from manned stations; defunct satellites.
- Rocket stage explosion: discarded rocket stages may also fragment explosively if remnants of their hypergolic fuel accidentally mixes. Delta rocket stages were particularly prone to this. Other rocket stages to have broken up include an Ariane upper stage in 1986 (Johnson and McKnight, 1987, p22), and the Pegasus HAPS, billed as the worst satellite breakup on record, producing up to 7×10^6 objects 1mm in size (Matney *et al*, 1997). Debris from an Ariane upper stage fragmentation in 1986 collided with the UK CERISE microsatellite in 1996.
- Gradual deterioration of satellite by atomic oxygen degradation of body parts.
- Deliberate break-up of satellites due to self-destruct modes and anti-satellite tests.
- Unknown causes of rocket stage fragmentations.

Sinks

- Atmospheric drag; Objects in low Earth orbit ("LEO") experience a small but non-negligible drag force from the upper reaches of the atmosphere which are sufficient to de-orbit them over a time period characteristic of the orbital altitude. Objects in higher orbit have longer lifetimes on the order of hundreds to thousands of years, while those in LEO may have a lifetime of just days (King-Hele, 1964).
- Solar/lunar tides: these affect only those satellites in highly eccentric orbits

such as those for geostationary transfer orbit* ("GTO") and Molniya orbits (Johnson & McKnight, 1987), (Reynolds et al, 1997).

- Radiation pressure: affects large area-to-mass ratio particles such as paint flakes.
- Deliberate removal: retrievable payloads such as the Long Duration Exposure Facility (LDEF) and the EUropean REtrievable CArrier (Eureca), defunct satellites returned via Space Shuttle or deorbited (Progress craft).

Of increasing concern to the space community is the proliferation of plans for large LEO constellations of telecommunications satellites - for example Motorola's Iridium constellation of 66 satellites, recently completed. Other projected schemes include the Globalstar constellation of 48 satellites at 1410km, and that of Teledisc, which aims to place over 800 satellites in 700km LEO (Swinerd et al, 1997).

The fear is that a critical state may be reached at some point where the collision frequency rises as a result of the increased number of debris particles in orbit, and as each collision creates new particles as ejecta fragments, the process becomes a self-sustaining chain reaction or cascade effect raising debris population density to levels were a satellite could be disabled by impact within months or even weeks of deployment (Barrows et al, 1995).

To this end, mitigation efforts are now underway by all spacefaring nations, and involve:

- Use of batteries with low risk of explosion (Penney, 1997), (Chekalin et al, 1997).
- Tethering of separation devices (Reynolds et al, 1997)
- Passivation of upper stages (opening of pressurised fuel tanks to allow the fuel to evaporate and prevent catastrophic fragmentation in the event of hypervelocity impact) (Bonnal et al, 1997).
- Reducing perigee of eccentric GTO orbits (Klinkrad, 1998)

* An eccentric orbit where the closest point is a few hundred km from the Earth's surface, whereas the furthest point is nearly 36,000km from the surface. More details in chapter 4.

1.2 Debris Environment Characterisation and Modelling

Two methods exist to characterise the debris environment: in-situ measuring, and remote detection, either by optical or radar means. In-situ measurement involves the deployment and return of space-flown surfaces for analysis on the ground, or by the telemetry of debris hits recorded on board the satellite.

Remote sensing involves either radar or optical means. Radar systems are able to obtain range and range-rate information on the objects detected to assist in orbit determination. The disadvantage with the system is the $1/r^4$ fall-off in returned signal power. Optical systems on the other hand cannot obtain range information, but the fall-off is only $1/r^2$ as the source of illumination is constant (the Sun). This is illustrated graphically in Figure 1.2. An extensive review of optical debris observations is given by Potter (1995).

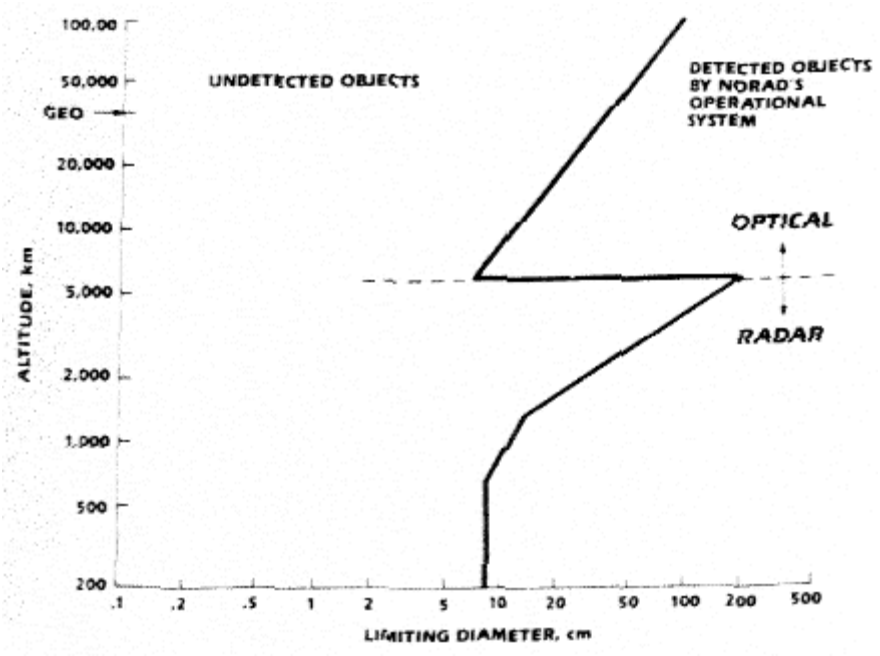

Figure 1.2: Sensitivity to space debris with height of the radar and optical systems of the North American Aerospace Defence Command (NORAD). From Kessler (1991).

1.3 Debris Particle Characteristics

Detection capability of debris depends not only on size but its shape and optical surface characteristics of the debris.

1.3.1 Debris size, mass

Debris size can range from whole rocket bodies to microscopic particles a few microns in diameter seen to penetrate foils left in orbit (McDonnell et al, 1997). Experimental data conducted with impacts into targets on the ground and collection and analysis of the debris fragments show that the cumulative mass distribution follows the empirically derived exponential function:

$$N = N_o \exp\left[-c\, m_f^{\frac{1}{2}}\right], \qquad (1.1)$$

where N = the number of fragments of mass greater than or equal to m_f, N_o = the total number of fragments, c is a constant governing the steepness of the slope of the curve, and m_f = the mass of fragment. Both c and N_o increase with impact energy, implying the ratio of small to large fragments increases as well as the total number of fragments produced (Johnson and McKnight, 1987, pp 33-34). Hence the number of smaller particles is believed to be orders of magnitude greater than those of larger size, as seen in Table 1.1 (Klinkrad, 1998).

	Number of debris particles	
Orbit regime (km)	size < 10cm	size > 10cm
h < 2000	10^{10}	15,100
2000 < h < 34786	7.8×10^{10}	2218
34786 < h <36786	9.81×10^{8}	949

Table 1.1: Relative numbers of differently-sized debris particles in Earth orbit.

1.3.2 Debris shape

The actual shape of space debris is not well investigated - studies usually concentrate on the impact potential of debris, yet shape dictates cross-sectional area (CSA) presented to the observer and therefore its optical characteristics (Madler, 1997). Shape also affects radar cross section, or RCS (Sato, 1994). Radar figures of RCS usually just combine a regular shape for the debris (disk, sphere) to calculate the mass, which often results in different sizes than those deduced by other means (Johnson and McKnight, 1987, p29).

Empirical studies of ground based impacts into test targets show that for objects with a CSA < $1m^2$ the shape becomes less irregular and more compact (Johnson and McKnight, 1987, P29). Hypervelocity impact test results held at the Arnold Engineering and Development Centre show the fragments produced as an elongated mass for the parent body whereas the smaller fragments have the shape of crushed boxes (Johnson and McKnight, 1987, pp34-37).

Radar studies of some centimetric debris (Sato, 1994) show an axial ratio implying a non-uniform shape exhibiting ellipsoidal characteristics, while radar imaging of larger objects with a resolution of 0.25m shows more structure.

A different mechanism other than collision or explosion is responsible for the relatively recently discovered population of centimetric droplets of liquid sodium and potassium coolant despatched from RORSAT nuclear-powered satellites at the end of their lifespan. Here, radar studies show that the particles are molten spherical droplets about 3 - 8cm in diameter (Sridhaven *et al*, 1997), (Meshcheryakov, 1997).

1.3.3 Debris Albedo

Deterioration of satellite materials from exposure to solar radiation and atomic oxygen are responsible for the breakup of spacecraft surfaces (Johnson and McKnight, 1987, p12), and therefore also cause changes to the surface optical properties of satellites and debris alike. The optical qualities of many common spacecraft materials have been extensively analysed in the hope of the data proving useful to debris identification (Culp & Gravseth, 1995).

Empirical measurements of the albedo of space debris have been made by Henize (1994) by comparing their RCS with optical observations. Results of the albedos measured are shown in Figure 1.3. The highest column in the histogram corresponds to a log albedo of -1.15, implying an albedo of 0.07.

These figures however are calculated assuming a lambert sphere at a phase angle of 90º. Elsewhere in this thesis the brightness of space debris at phase angles other than 90º are required, so the albedo for these angles is calculated too.

To achieve this the albedo at a phase angle of $\phi = 0º$ is specified (called the Geometric Albedo A_g), which is then multiplied by the appropriate phase function $\Phi(\phi)$, which for a lambert sphere is shown in equation (1.2) (Petri, 1975):

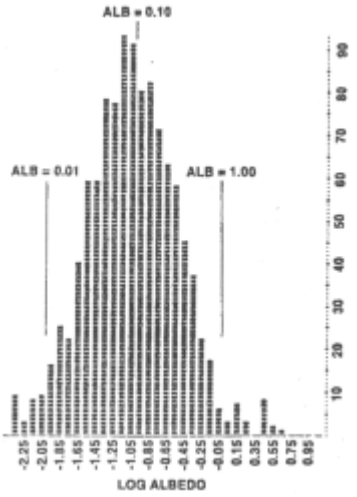

Figure 1.3: Log albedo of 1094 observations of space debris (Henize et al, 1994).

$$\Phi(\phi)_{\text{lambert}} = \frac{2}{3\pi}\left[\sin\phi + (\pi - \phi)\cos\phi\right]. \tag{1.2}$$

Hence the Bond Albedo is calculated as

$$A_b = A_g \ \Phi(\phi) \ . \tag{1.3}$$

The value of A_b given by Henize (1994) is used to calculate the value of A_g required to ensure that $A_b = 0.07$ for $\phi = 90^o$. At that phase angle, $\Phi_{90} = 2/(3\pi)$, therefore:

$$A_g = 3\pi A_b / 2 = 0.3299 \ . \tag{1.4}$$

Thus the general term for the Bond albedo of the debris particles at a phase angle ϕ is calculated as:

$$A_b(\phi) = 0.3299\frac{2}{3\pi}\left[\sin(\phi) + (\pi - \phi)\cos(\phi)\right]. \tag{1.5}$$

A polar plot of the albedo for the model debris particle is shown in Figure 1.4.

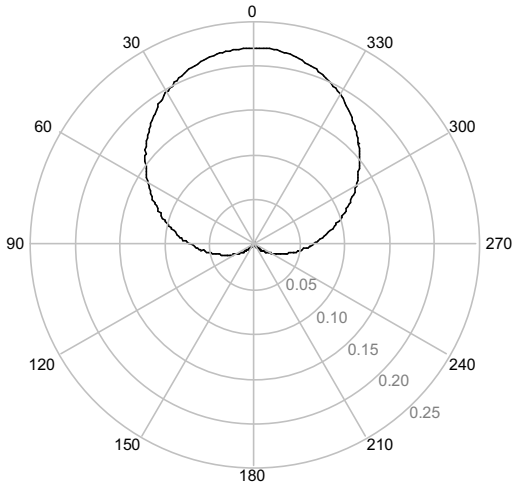

Figure 1.4: Polar plot of phase function for a lambert sphere.

1.4 Structure of Thesis

This thesis looks at two aspects of the problem of ground-based optical space debris detection. It is divided roughly into two parts: the first part looks at the visibility of certain types of debris orbit under various conditions and ascertains the choice of telescope pointing direction to optimise detection rates. The second part presents a computer program to enable detection of faint debris particles in real time (i.e. while the debris is passing through the field of view of the telescope), with very low signal-to-noise (SNR) ratios.

A chapter-by-chapter breakdown of the thesis is as follows:

1. This chapter
2. Discussion of the possible range of angular speeds apparent to an observer on the Earth's surface - a value different from its angular velocity with respect to the centre of the Earth and dependent on both debris and observer location, orbit eccentricity and inclination, and where in the orbit the debris is observed. This data helps to characterise the regime within which a detection algorithm (presented in chapters 7-9) must operate.
3. Introduction to the investigation into optimisation of debris detection with telescope pointing direction, and an introduction to the "SkyPlot" program developed by the author to furnish information on this subject.
4. Details of the SkyPlot program; its structure, and the physical and astronomical factors considered in the model.
5. Results of the SkyPlot model, and conclusions.
6. Introduction to the debris detection "DDT" program; i.e. the design drivers of speed and imagery under which it must operate.
7. Details of the DDT program, its structure, etc.
8. Tests of the DDT performance and runs with real telescope images, plus a discussion of minimum debris diameter detectable.
9. Main conclusions from both parts, and further suggestions, including a discussion on how the DDT program could be adapted to search for asteroids.